XLI CILAMCE
XLI Ibero-Latin American Congress on Computational Methods in Engineering
16-19 November, 2020 FOZ DO IGUAÇU PARANÁ - BRAZIL

Machine-precision fracture mechanics evaluations with the consistent boundary element method

Osmar Alexandre do Amaral Neto[1], Ney Augusto Dumont[1]

[1]*Department of Civil and Environmental Engineering, Pontifical Catholic University of Rio de Janeiro*
Rua Marquês de São Vicente, 225, 22451-900, Rio de Janeiro, Brazil
osmaralexandre22@hotmail.com, dumont@puc-rio.br

Abstract. As hitherto proposed in the technical literature, the boundary element modelling of cracks is best carried out resorting to a hypersingular fundamental solution. A more natural approach might rely on the direct representation of the crack tip singularity, as already proposed in the frame of the hybrid boundary element method. However, recent mathematical assessments indicate that the conventional boundary element formulation – based on Kelvin's fundamental solution – is in fact able to precisely represent high stress gradients and deal with extremely convoluted topologies. We propose in this paper that independently of configuration a cracked structure be geometrically represented as it would appear in real-world laboratory experiments, with crack openings in the range of micrometers or less. Owing to a newly developed integration scheme for two-dimensional problems, machine precision evaluation of all quantities may be achieved and stress results consistently evaluated at interior points arbitrarily close to crack tips. Importantly, no artificial topological issues are introduced and linear algebra conditioning is kept under control. Some numerical illustrations show that highly accurate results are obtained for cracks represented with just a few quadratic, generally curved, boundary elements and a few Gauss-Legendre integration points per element. The numerical evaluation of the J-integral turns out to be straightforward and actually the most reliable means of obtaining stress intensity factors.

Keywords: Boundary element method, Fracture mechanics, Stress intensity factor, J integral

1 Introduction

Fracture mechanics phenomena have being systematically investigated since the seminal studies by Inglis [1] in the year 1913, who proposed the analysis of stress concentration around straight cracks in plane plates. Griffith [2] introduced in 1920 thermodynamics concepts to formulate a fracture mechanics theory based on *energy balance*. Later on, Irwin extended Griffith's ideas to metals and proposed the concept of *energy release rate* [3] and, on the basis of the developments by Westergaard [4], also the *stress intensity factor* (SIF) [5] as a measure to be definitely considered in the fracture mechanics theory. In the year 1968, Rice [6] showed that the energy release rate may be obtained by means of a line integral, for two-dimensional (2D) problems, which became known at the *J-integral*. The application of these concepts to a practical problem depends of the adequate evaluation of the stress state around a crack tip. The first boundary element development in the field may be attributed to Cruse in the year 1971 [7]. However, owing to space restrictions we should not carry out a literature review on the subject.

The second author and previous collaborators have already in part successfully arrived at an attempt on the basis of the *hybrid boundary element method* to adequately represent the stress field around a crack tip in terms of Williams' series as well as of generalizations of Westergaard's stress functions [8–10].

More recently, a consistent formulation – actually a both conceptually and numerically long due correction – of the conventional, *collocation boundary element method* (CBEM) was proposed [11, 12], according to which a convergence theorem could be envisaged and the evaluation of results has turned out achievable within machine precision for internal points arbitrarily close to an elastic body's boundary regardless of topology issues. The numerical implementation considers arbitrarily high-order boundary elements for 2D bodies of any shape and topology as well as flat boundary elements of a three-dimensional body. The application of this consistent formulation to 2D fracture mechanics problems was the subject of the first author's M.Sc. thesis [13], which showed that a generically curved crack may be numerically simulated exactly as if in a real-life experimentation, with the faces distinctly modelled for arbitrarily small openings as long as the continuum mechanics is dimmed applicable.

2 The consistent boundary element method

As applied to an elastostatics problem, boundary nodal displacements $\mathbf{d}$ and traction attributes $\mathbf{t}$ are interrelated by means of the single-layer and double-layer potential matrices $\mathbf{G}$ and $\mathbf{H}$ as

$$\mathbf{H}(\mathbf{d} - \mathbf{d}^p) = \mathbf{G}(\mathbf{t} - \mathbf{t}^p) \tag{1}$$

In this equation, it is also considered that body forces may be at least approximately expressed in terms of equivalent nodal displacements $\mathbf{d}^p$ and boundary traction parameters $\mathbf{t}^p$, which is not always a simple task [11–13]. This equation turns out to be an application of *Somigliana*'s identity that converts boundary data into domain displacements. Whenever the boundary data are inaccurate, as the result of approximated values of $\mathbf{d} \equiv d_f$ and $\mathbf{t} \equiv d_\ell$ for a given problem as well as of the piecewise boundary interpolation, an error term $\boldsymbol{\epsilon}$ should actually be added to this equation [11, 12]. The matrices $\mathbf{G}$ and $\mathbf{H}$ are expressed in terms of the boundary integrals

$$G_{s\ell} = \int_\Gamma u^*_{is}(\mathbf{x} - \mathbf{x}_s) t_{i\ell}(\mathbf{x}) \mathrm{d}\Gamma(\mathbf{x}) \tag{2}$$

$$H_{sf} = \int_\Gamma \sigma^*_{jis}(\mathbf{x} - \mathbf{x}_s) n_j(\mathbf{x})\, u_{if}(\mathbf{x}) \mathrm{d}\Gamma(\mathbf{x}), \tag{3}$$

where $u^*_{is}(\mathbf{x} - \mathbf{x}_s)$ and $\sigma^*_{jis}(\mathbf{x} - \mathbf{x}_s)$ are the displacement and stress (Kelvin's) fundamental solutions of the elastic problem – which have global support – and $\Gamma(\mathbf{x})$ is the integration boundary. In the above equation and in the following, repeated indices mean summation. The vector $\mathbf{x} \equiv (x, y, z)$ stands for the Cartesian coordinates of a given point, in the case a field point, and $n_j(\mathbf{x}(\xi, \eta))$ are the Cartesian components of the unity outward vector $\vec{n}(\mathbf{x}(\xi, \eta))$ to $\Gamma(\mathbf{x}(\xi, \eta))$, in terms of parametric variables (ξ, η), for a general 3D problem. The subscript s refers to a given source node (at which the unit point force of the singular fundamental solution is applied) and the subscripts f (which stands for field) and ℓ (also a field reference) indicate respectively to which node or surface point the displacement-interpolation function $u_{if}(\mathbf{x}(\xi, \eta))$ or the traction-interpolation function $t_{i\ell}(\mathbf{x}(\xi, \eta))$ -– both with local support -– are referred. $u_{if}(\mathbf{x}(\xi, \eta))$ comes from the piecewise interpolation of displacements $u_i(\mathbf{x}(\xi, \eta))$ along the boundary, $u_i(\mathbf{x}) = u_{if}(\mathbf{x}(\xi, \eta))d_f$, where d_f are the nodal displacements. In a practical finite element or boundary element implementation, $u_{if}(\mathbf{x}(\xi, \eta))$ is actually represented by polynomial shape functions $N_f(\xi, \eta)$:

$$u_{if}(\mathbf{x}(\xi, \eta)) = \begin{cases} N_f(\xi, \eta) & \text{if } i \text{ and } f \text{ refer to the same Cartesian direction} \\ 0 & \text{otherwise} \end{cases} \tag{4}$$

In the expression of $\mathbf{H}$, the Jacobian used in the definition of $n_j(\mathbf{x}(\xi, \eta))$ cancels out with the Jacobian of $\mathrm{d}\Gamma(\mathbf{x}) = |J(\xi, \eta)|\, \mathrm{d}\xi \mathrm{d}\eta$. For the single-layer potential matrix $\mathbf{G}$, it is proposed that the usual (as found in the literature) interpolation polynomials $t_{i\ell}$ of traction forces in eq. (2) be replaced with

$$t_{i\ell}(\mathbf{x}(\xi, \eta)) = \frac{|J|_{(\text{at } \ell)}}{|J|} \begin{cases} N_\ell(\xi, \eta) & \text{if } i \text{ and } \ell \text{ refer to the same Cartesian direction} \\ 0 & \text{otherwise} \end{cases} \tag{5}$$

where $|J|_{(\text{at } \ell)}$ is the value of the Jacobian at the point characterized by the subscript ℓ [11, 12]. Nothing changes formally in the development of the BEM for curved boundary segments (and, of course, nothing changes numerically for the trivial cases of straight or flat boundary segments), except that the evaluation of $\mathbf{G}$ becomes much easier and actually more consistent as compared to proposed implementations given in the technical literature. In fact, $|J|$ cancels out in the product $t_{i\ell}\mathrm{d}\Gamma$ in eq. (2) for $t_{i\ell}$ defined as suggested, and the integrand of $\mathbf{G}$ becomes a polynomial that multiplies the assumed kernel u^*_{is}.

2.1 A brief outline of the numerical integration issues

As proposed above, the integrands in eq. (2) are given as products of the kernels with polynomial terms regardless the element order for either 2D or 3D problems. For 2D problems, it has been shown that boundary elements of any shape may be dealt with in a unified procedure that enables machine precision results for the evaluation not only of $\mathbf{G}$ and $\mathbf{H}$ but also for displacement and stress results at internal points – in the latter case allowing for eventual quasi hypersingularities – no matter how close source and field points may be to each other.

The outline of the numerical evaluation procedures is out of scope in the present developments, but it may be worth illustrating in Fig. 1 the kinds of singularity that must be taken into account. For the cubic element of the figure, given in terms of the parametric variable $\epsilon \in [0, 1]$, an actual singularity occurs for the source point at A, thus for $0 \leq \epsilon \leq 1$. For the source point at B, represented by $\epsilon > 1$ but still close to the integration interval,

the integrals of eq. (2) must be dealt with for the special case of a real quasi-singularity. On the other hand, if the source point is at C, its complex location $\epsilon = a \pm ib$ must be found for the correct consideration of the corresponding procedure [12, 14].

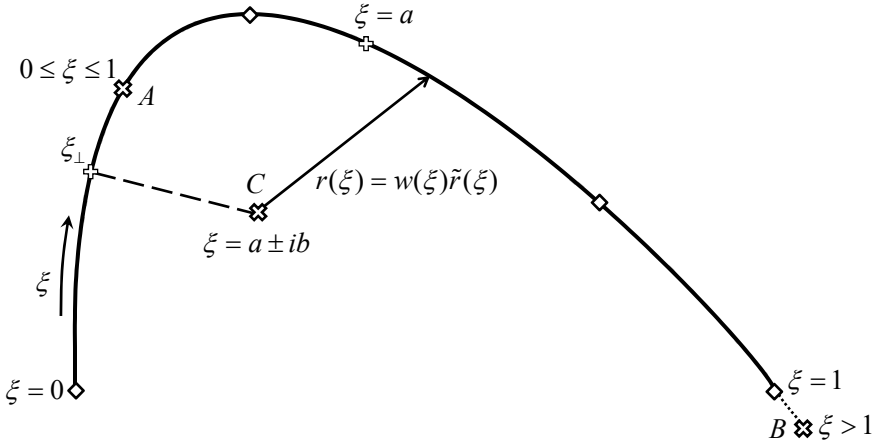

Figure 1. Illustration of actual (A) and real (B) or complex (C) quasi singularity poles

3 Illustrative numerical assessments of two fracture mechanics problems

A few plane stress problems are assessed next. Unless otherwise specified, we consider a material with transversal elasticity modulus $G = 80,000$ units of stress and Poisson's ratio $\nu = 0.2$. All singularity and quasi-singularity cases are evaluated within machine precision, but the use of $n_g = 4$ Gaussian points for the regular integrals leads to final precision of results that cannot be better than 10^{-7}. In fact, several numerical assessments conducted using 4, 6 and 8 Gaussian points combined with 20, 30 and 40 precision digits implemented in the Maple software showed that all results of interest could be obtained within a precision of 10^{-5} for $n_g = 4$ points and 30 digits [13], which will be used here for all regular integrals along generally curved quadratic elements. Stress intensity factors are evaluated in terms of J-integrals along circles centred at the crack tip, subdivided into 10 sectors and also using $n_g = 4$ Gaussian points per sector.

3.1 Analysis of an elliptic crack in the open domain

The simplest and best representative case of fracture mechanics is the one of a straight crack in the open domain for a constant stress state applied transversally to the crack at infinity, with stress disturbances to be assessed at the crack's tips and mode I stress intensity factor to be evaluated. We represent this crack with length $2a = 2$ units and already as an elliptic opening with $2b = 2 \times 10^{-3}$ units, which would only exactly correspond to the problem originally proposed and solved by Westergaard [4] in the limit case of $b \to 0$.

In eq. (1), this case corresponds to a far field stress state σ^p_{ij} evaluated as traction parameters $\mathbf{t}^p$ and nodal displacements $\mathbf{d}^p = \mathbf{0}$ at the crack borders. Moreover, the occurrence of the crack implies that $\mathbf{t} = \mathbf{0}$, so that eq. (1) directly leads to the solution of the crack borders' nodal displacements $\mathbf{d}$ as

$$\mathbf{d} = -\mathbf{H}^{-1}\mathbf{G}\mathbf{t}^p \tag{6}$$

since $\mathbf{H}$ is non-singular for an open domain problem, although we might expect some ill-conditioning due to the proximity of the crack faces: the present numerical implementation has brilliantly passed this test [13]. After evaluation of $\mathbf{d}$, results at internal points are obtained by using Somigliana's identity, with final stress values given as the superposition with the applied far-field particular solution σ^p_{ij}.

A convergence study is shown in Fig. 2 for errors in the numerical evaluation of the stress intensity factor as compared with the analytical result $K_I = \sigma\sqrt{\pi a} \approx 1,7724539$, for different numbers of quadratic elements along the crack faces. Since the implemented code does not take advantage of the double symmetry of the problem, the number of elements per half crack face is a quarter of the indicated values. The node spacing along the crack varies geometrically from crack tip to the center according to the indicated ratios, for the three cases analysed. We see that agglutinating the nodes close to the crack tip (ratio = 1.5) does not necessarily lead to better results, which are for ratio = 1.35, with errors tending to 10^{-4}. This is mainly related to the geometric approximation

of the assumed elliptic initial crack shape in terms of successive quadratic segments, which provoke an undesired angulation between adjacent elements instead of a smooth surface. In order to assess how the size of the elliptic

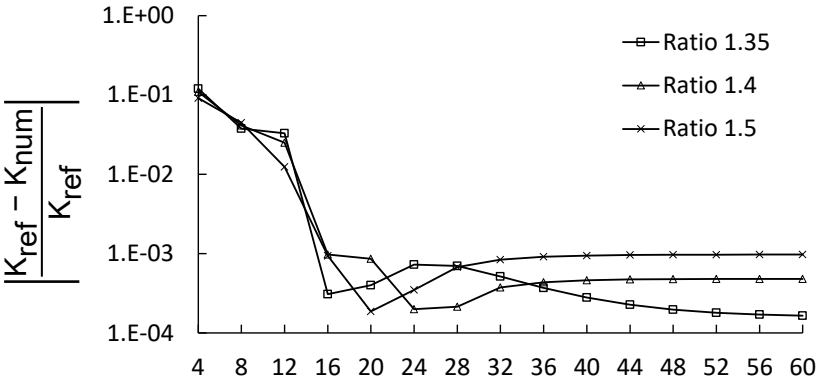

Figure 2. Errors in the evaluation of SIF values for the crack with initial opening 2×10^{-3}

minor axis affects results, Fig. 3 shows relative errors in the evaluation of SIFs for $b = 10^{-3}$, 10^{-4} and 10^{-5} units for different ratios in the geometric increase of node spacing from tip to middle of the crack. There is a tendency to arrive at the SIF for the fracture mechanics theory, although the angulation between adjacent elements causes too much disturbance: best result is the error of about 10^{-6} for opening $b = 10^{-5}$ with internode space increasint ratio 1.1. The angulation between adjacent quadratic elements, as implemented in this simulation, may be measured in

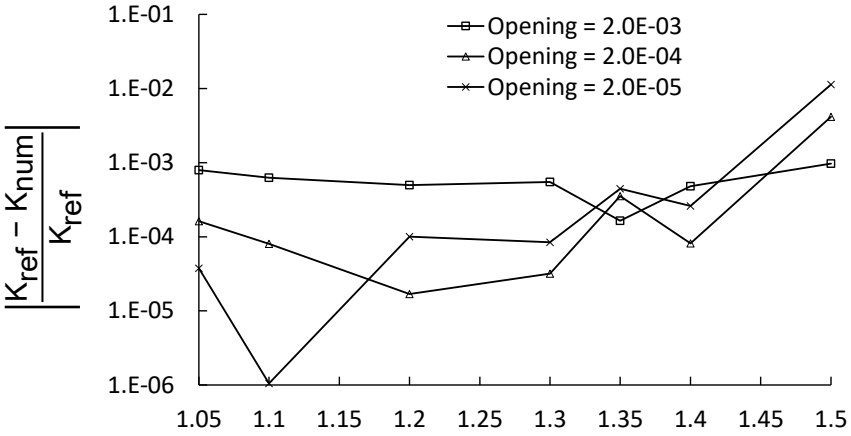

Figure 3. Errors in the evaluation of SIF values for the crack with different assumed initial openings

terms of how much the discontinuous part of the matrix **H** for an interelement node differs from 0.5, which is the value for a smooth surface. Since all singular evaluations are carried out within machine precision, this deviation from 0.5 is a reliable account of the introduced geometry errors. This is shown in Fig. 4 for two different internodes space increasing ratios in the case of the half opening $b = 10^{-5}$ and a total of 60 quadratic elements in the crack discretization, which corresponds to 31 nodes from tip to a face's middle (the values for the internal nodes, given by even numbers, are of course exactly 0.5). The geometry errors are not large, in general, and smaller for nodes not too differently spaced, but larger at the crack's tip, where such discrepancy should better be avoided. The conclusion is that results in the values of the SIF cannot be expected to improve unless this angulation issue is adequately solved. There is indeed a study in progress on this subject with promising initial results.

Figure $5(a)$ presents normal stress results at 40 points spaced at geometrically increasing distances r/a along a straight line extending from the crack tip, as obtained for the discretization with $b = 10^{-3}$ and 60 elements with internodes spacing ratio 1.35, and compared with the reference values according to Westegaard's developments. It is worth observing the $1/\sqrt{r}$ singularity tendency as the points get close to the crack tip. The comparison with the target results are better displayed in terms of the error norm of Fig $5(b)$, where both vertical and horizontal axes are in logarithmic scale. As assessed by Amaral Neto [13] for this case of an immersed straight crack as well as for some other crack configurations, the SIF results are actually dependent of the assumed Poisson's ratio, a fact that is in general ignored in the technical literature, maybe because the numerical differences are smaller than the built-in errors of the hitherto implemented simulations.

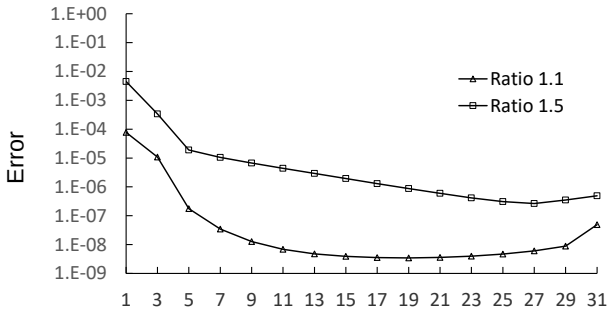

Figure 4. Geometry discretization errors measured in terms of the discontinous part of **H**

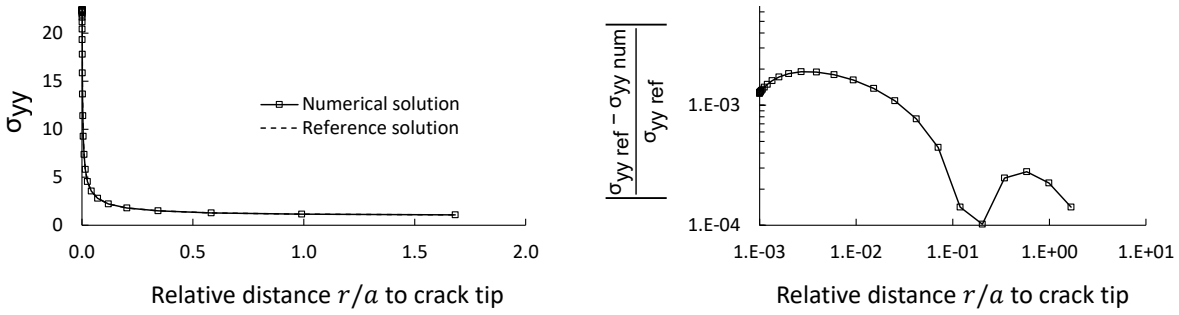

Figure 5. Normal stress values (a) and relative errors (b) at points along a line extending from the crack tip

3.2 Analysis of an inclined edge crack in a rectangular plate

The rectangular plate with an inclined edge crack of Fig. 6 (drawing not in scale) was examined by Amaral Neto [13] for a longitudinal constant load and edge openings 2×10^{-3}, as indicated, as well as 2×10^{-4} and 2×10^{-5}. The discretization of the four external edges consisted of a fixed number of 80 uniformly distributed quadratic elements. In the numerical analyses, the numbers of quadratic elements along each crack face varied from one to 15 and several internode space increasing ratios from crack tip to edge were applied, as described for the previous example. Overall results tended to be better when such ratios were not too large, but just about 1.2 to 1.3. The obtained results were quite insensitive to discretizations with more than four elements along each crack face. Stress intensity factor results were compared with the ones given by Tada and Irwin [15], whith difference errors of about 10^{-2} to 10^{-3} and more affected (although always slightly) by different Poisson's ratio than observed for the previous example. It is worth observing that our model is not exactly the one in Tada and Irwin's book, as we are considering a finite, although small, crack opening. Moreover, our results are likely to be more reliable, as there is no analytical solution for this problem.

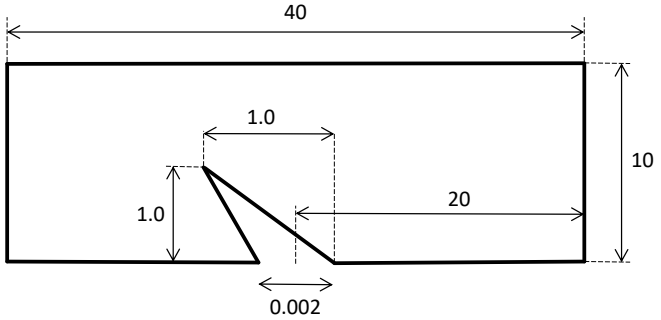

Figure 6. Inclined edge crack in a rectangular plate (drawing not in scale).

Since this is the case of a finite elastic body, a very objetive assessment of the implemented numerical solution may be undertaken. In fact, as already used by second author in several numerical investigations, Amaral Neto [13] submitted the plate of Fig. 6 to a family of displacement polynomials given of degrees one, two, three, four and five, a total of 20 polynomial fields (four for each degree) that are non-singular fundamental solutions of the

proposed elastic problem. For each polynomial, boundary displacements and traction forces can be evaluated and inserted into eq. (1) in order to check its accuracy both as stated in this equation as well as in terms of the system solution indicated in eq. (6) – after duly compensating for rigid body displacements [13]. In fact, while shear discretization accuracy can be assessed by means of eq. (1), the matrix inversion in eq. (6) makes possible to measure the eventual onset of ill-conditioning.

According to Dumont [14], the numerical results are expected to be accurate within machine precision for linear displacement fields. (It would be the case for quadratic displacement fields, as well, if the borders were given by straight segments, which is strictly speaking not the case here, as the crack face nodes are not evenly spaced inside a quadratic boundary element.) Since the regular parts of the integrals are evaluated numerically, the expected global results cannot be more accurate than the quadratures allow for. Figure 7 shows error results for eq. (1), $|\mathbf{Gt_{pol}} - \mathbf{Hd_{pol}}|$, as well as for (6), $|\mathbf{d_{pol}} - \mathbf{d_{num}}|$, in the cases of crack openings $2 \cdot 10^{-3}$, on the left, and $2 \cdot 10^{-5}$, using 4, 6 and 8 quadrature points. The horizontal axes show average results for the four polynomials of each degree used in the analyses. The results for the first-degree polynomials – for which analytical results are expected – are multiplied by some constants in order to keep the graphics within a reasonable interval. It is expected that errors increase as the polynomial degrees increase. In fact, as the quintic polynomials, for instance, give rise to overall high stress gradients, the displayed results are a threshold of the accuracy we should expect in the fracture mechanics assessments. It is worth observing some ill-conditioning related to eq. (6) – which increases as the crack opening gets smaller – but way below the approximation errors.

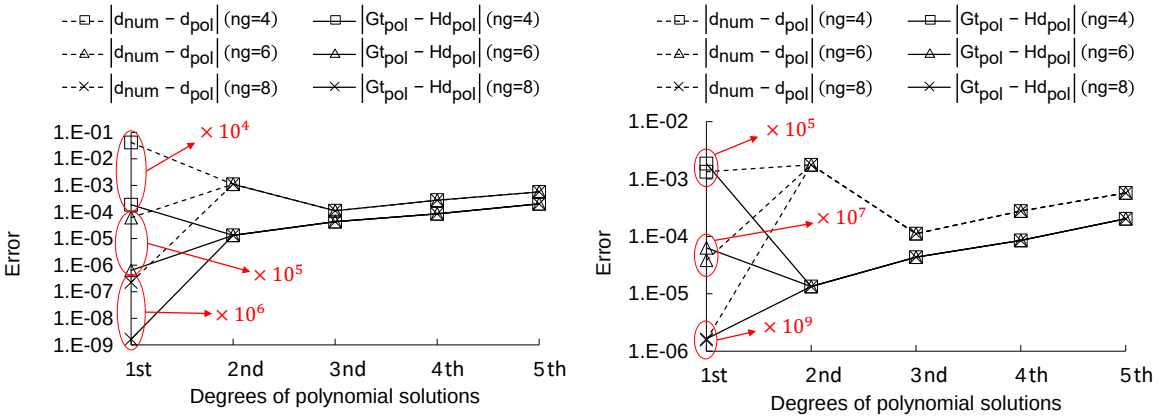

Figure 7. Errors related to eqs. (1)and (6), for the plate of Fig. 6 with crack openings $2 \cdot 10^{-3}$ (a) and $2 \cdot 10^{-5}$ (b)

4 Conclusions and prospective works

It has been shown that a code implementation of the consistent, *collocation boundary element method* can be used to analyze crack configurations of the 2D fracture mechanics as they are expected to exist in real life. In this code, a unified integration scheme deals with singularities and quasi-singularities of an arbitrary degree of severity, as source and field points can be infinitely close to each other, the only limitation being the machine's capability of representing numbers – thus avoiding round-off errors. One might think of working with a code that combines Kelvin's singular and hypersingular fundamental solutions to model a crack's face and its oposite, respectively, a classical usage to represent cracks of zero opening. The present code actually already allows for such simulation, as the evaluation of stress results at internal points deals with quasi hypersingularities within machine precision. However, modelling real crack configurations opens up the possibility of implementing a procedure to investigate the crack propagation phenomenon from its onset and during successive steps of the crack becoming wider and larger – and eventually kinking and bifurcating. The combination with cohesive elements is also quite natural in the present code implementation.

An issue investigated in the example of Section 3.1 are spurious angulations between adjacent elements in the attempt to represent an elliptic geometry as a succession of quadratic elements – aggravated at the proximity of the crack tip, as some stress disturbance is unwillingly introduced. (An isogeometric implementation is not a solution, as the consistent BEM must rely on an isoparametric formulation [12]). The main concern is however how to assume the shape of an unloaded crack in a real sample other than making local measurements and just trying to have representative models. Westergaard proposed a straight crack with initial zero opening, for which a far-field constant stress state is analytically shown to cause an elliptic opening. This is the reason to suppose

in Section 3.1 that the unloaded straight crack is elliptic with minor axis tending to zero. In the configuration for $a = 10^{-3}$ the distance between opposite nodes closest to the crack tip is as small as 1.8×10^{-5} for the model with 60 boundary elements. The assumption of a straight edge crack of Fig. 6 seems quite reasonable, but the linear narrowing from the edge to the tip is also in need of justification. In such a case there were no spurious angulations and the crack tip is very narrow indeed: for the configuration with the indicated opening 2×10^{-3} and a total of 30 boundary elements the distance between opposite nodes closest to the crack tip is 8.6×10^{-8}, which is already going beyound the continuous mechanics assumptions but is still doable mathematically.

A possibility that is already under investigation is the modelling of the crack as arbitrarily close, parallel (or not) interfaces interconnected by curved transition elements that preserve surface smoothness wherever required (this is done by just adjusting the loci of the internal element nodes). The simplest case of the straight crack of Section 3.1 would be modelled as in Fig. 8, for quadratic, cubic or quartic boundary elements.

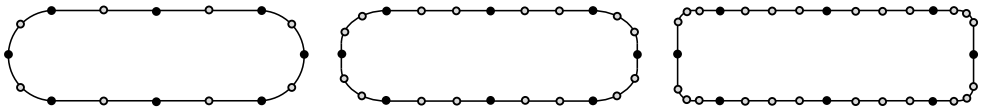

Figure 8. Newly proposed models of a straight crack with quadratic, cubic and quartic boundary elements

The model proposed in this figure seems to enable a friendlier manipulation of the numerical simulations as a crack propagates and eventually kinks or bifurcates. This is the subject of a research work in progress.

Acknowledgements. This project was supported by the Brazilian agencies CAPES and CNPq.

Authorship statement. The authors hereby confirm that they are the sole liable persons responsible for the authorship of this work, and that all material that has been herein included as part of the present paper is either the property (and authorship) of the authors or has the permission of the owners.

References

[1] Inglis, C. E., 1913. Stress in a plate due to the presence of cracks and sharp corners. *Transactions of the institute of Naval Archtects*, vol. 55, pp. 219–241.
[2] Griffth, A. A., 1920. The phenomena of rupture and flow in solids. *Philosophical Transactions*, vol. 221, pp. 163–198.
[3] Irwin, G. R., 1956. Onset of fast crack propagation in high strength steel and aluminum alloys. *Sagamore Research Conference Proceedings*, vol. 2, pp. 289–305.
[4] Westergaard, H. M., 1939. Bearing pressures and cracks. *Journal of Applied Mechanics*, vol. 6, pp. 49–53.
[5] Irwin, G. R., 1957. Analysis of stresses and strains near the end of a crack traversing a plate. *Journal of Applied Mechanics*, vol. 24, pp. 361–364.
[6] Rice, J. R., 1968. A path independent integral and the approximate analysis of strain concentration by notches and cracks. *Journal of Applied Mechanics*, vol. 35, pp. 379–386.
[7] Cruse, T. A. & Van Buren, W., 1971. Three dimensional elastic stress analysis of a fracture specimen with an edge crack. *International Journal for Fracture Mechanics*, vol. 7, pp. 1–15.
[8] Dumont, N. A. & Lopes, A. A. O., 2002. On the explicit evaluation of stress intensity factors in the hybrid boundary element method. *Fatigue & Fracture of Engineering Materials & Structures*, vol. 26, pp. 151–165.
[9] Dumont, N. A. & Mamani, E. Y., 2011. Generalized Westergaard stress functions as fundamental solutions. *CMES – Computer Modeling in Engineering & Sciences*, vol. 78, pp. 109–150.
[10] Dumont, N. A., Mamani, E. Y., & Cardoso, M. L., 2018. A boundary element implementation for fracture mechanics problems using generalized Westergaard stress functions. *European Journal of Computational Mechanics*, vol. 27:5-6, pp. 401–424.
[11] Dumont, N. A., 2010. The boundary element method revisited. *Boundary Elements and Other Mesh Reduction Methods XXXII*, vol. 50, pp. 227–238.
[12] Dumont, N. A., 2018. The collocation boundary element method revisited: Perfect code for 2D problems. *International Journal of Computational Methods and Experimental Measurements*, vol. 6, pp. 965–975.
[13] Amaral Neto, O. A., 2020. Consistent application of the boundary element method to fracture mechanics problems (in Portuguese). Master's thesis, PUC-Rio, Rio de Janeiro, Brazil.
[14] Dumont, N. A., 1994. On the eficient numerical evaluation of integrals with complex singularity poles. *Engineering Analysis with Boundary Elements*, vol. 13, pp. 155–168.
[15] Tada, H., Paris, P. C., & Irwin, G. R., 2000. *The Stress Analysis of Cracks Handbook*. ASME Press.